AIAA JOURNAL
Vol. 44, No. 2, February 2006

Numerical Study of Detonation Stabilization by Finite Length Wedges

Miguel A. T. Walter* and Luís Fernando Figueira da Silva†
Pontifícia Universidade Católica do Rio de Janeiro, 22453-900 Rio de Janeiro, Brazil

A numerical study is conducted of the interaction between the leading oblique detonation wave stabilized by a wedge ramp of finite length and the expansion waves generated by the sudden deflection of the wedge surface. The two-dimensional Euler equations for a reactive gas mixture are solved using a cell-centered finite volume technique on unstructured meshes. Mesh refinement and coarsening techniques are used to concentrate the computational volumes in regions of interest of the flowfield. A detailed chemical kinetic mechanism is employed to describe the combustion process in the mixtures of hydrogen and air considered. Computational results show that a Chapman–Jouguet oblique detonation wave is obtained for intermediate wedge angles within the range of stable detonations. For wedge angles near to the maximum angle that supports stable oblique detonations, decoupling of the oblique detonation wave is observed.

I. Introduction

THE development of ram accelerators[1] and supersonic combustion ramjets[2] leads to the study of the interaction between compressibility effects and the combustion process in high Mach number flows.[3] In particular, this interaction may result in the onset of oblique detonation waves, which may arise when the former system is operating at speeds higher than the detonation velocity of the combustible mixture,[4] and, in the latter, when oblique detonation wave engines are considered.[5] Previous works have shown that overdriven oblique detonation waves may be stabilized when a wedge interacts with a supersonic reactive gas mixture.[6,7] From the point of view of the combustion process, oblique detonation waves (ODW) convert high-speed fresh unburned reactants to products in distances that do not exceed 1 mm for most gas mixtures,[8] albeit with a substantial increase in entropy, which is due mostly to the leading oblique shock wave. Among all oblique detonation waves that may be stabilized in a given gas mixture, the one leading to the smallest entropy increase is a Chapman–Jouguet (C–J) ODW. Moreover, this detonation wave is isolated from downstream perturbations by a sonic surface, which further increases its interest for propulsion applications.

The aim of this work is to evaluate freestream conditions and wedge angles that may lead to the formation of a wedge-stabilized C–J ODW. The onset of such a wave is sought through the interaction between an overdriven ODW and expansion waves. Figure 1 shows the geometry of interest, which consists of a wedge ramp, followed by a sudden deflection of the wedge surface that turns the wedge surface parallel to the freestream flow and limits the ramp length. The oblique shock wave stabilized over the ramp triggers combustion and thus leads, after a transition region, to an overdriven ODW. This ODW subsequently interacts with the expansion fan generated by the deflection of the ramp surface. This figure schematically shows one possible flow structure resulting from this interaction.

Analytical studies based on Rankine–Hugoniot relations together with equilibrium chemistry[9,10] give conditions to stabilize oblique detonation waves over a wedge. Results of this analysis can be represented by polar diagrams. A typical one is shown in Fig. 2, which emphasizes that there is a range of flow deflection angles (δ_{cj}, δ_{max}) where oblique detonation waves may be stabilized and remain attached to the wedge. For flow deflection angles larger than δ_{max}, only detached curved detonation waves are expected. Below this range, $\delta < \delta_{cj}$, weak ODW would occur. Detonations with angles greater than θ_{max} seem to be of little interest to propulsion applications because the downstream flow is subsonic and a large entropy increase results.

Numerical studies that involved nonequilibrium chemical kinetic mechanisms[6,7] made it possible to investigate the flow structure of overdriven oblique detonation waves attached to a wedge. This structure consists of an oblique shock wave (OSW), an induction region, followed by a transition region and an oblique detonation wave that emanates from a triple point. Three different transition regimes from the oblique shock wave to the oblique detonation wave have been obtained.[11]

Experimental studies[10,12] using an oblique detonation tube investigated the different possible combustion regimes when the ODW is supported by a gaseous wedge. Expansion tube studies,[13] which considered wedge angles greater than the maximum wedge angle allowed for attached detonations, also led to the onset of ODW, although the steadiness of the flowfield could not be assessed. Comparison between computational and experimental results[14] shows that the overall flow structures obtained are in good agreement, and that induction time controls the OSW/ODW transition, both in the computations and in the experiments.

As schematically shown in Fig. 1, once the ramp-stabilized oblique shock wave triggers combustion of the reactive mixture, leading to a stable overdriven oblique detonation wave, the expansion waves emanating from the deflection point intersect the leading overdriven oblique detonation wave. This interaction decreases the pressure, leading to progressive bending of the ODW by reducing its strength. As the ODW is weakened, the ODW angle is decreased from θ_{ODW} at the leading ODW to θ_R farther downstream. Simultaneously, in the interaction region, the Mach number and temperature downstream of the ODW are increased and reduced, respectively. Reduction in pressure and temperature downstream of the ODW leads to an increase on the induction time of the combustion process. Increments of the induction time and on the Mach number are responsible for an increase in the length of induction region of the chemical process. This region is situated between the leading OSW and the reaction front. The outcome of such an interaction is a priori unknown. A possible result of this interaction is that the leading ODW becomes a Chapman–Jouguet oblique detonation wave (C–J ODW). In such a case, the downstream Mach number normal to the wave reaches the sonic value, and further expansion of the

Presented as Paper 2004-3712 at the AIAA/ASME/SAE/ASEE 40th Joint Propulsion Conference, Fort Lauderdale, FL, 11–14 July 2004; received 23 July 2004; revision received 26 August 2005; accepted for publication 26 August 2005.

*Graduate Student, Department of Mechanical Engineering, Rua Marquês de São Vicente, 225.

†Visiting Professor, Department of Mechanical Engineering, Rua Marquês de São Vicente, 225. Senior Member AIAA.

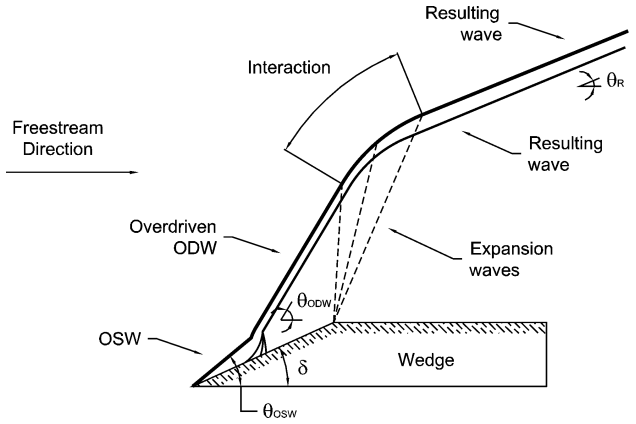

Fig. 1 Schematic representation of interaction between an overdriven oblique detonation wave and expansion waves.

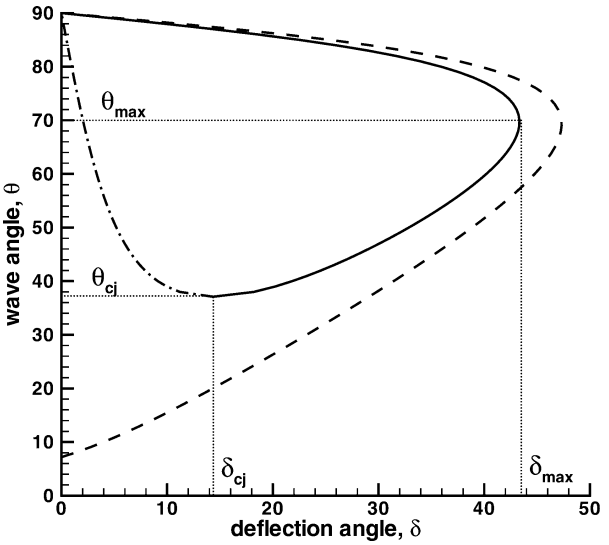

Fig. 2 Shock and detonation wave polars for $M_\infty = 8$, $p_\infty = 0.75$ atm: - - - -, OSW; ——, overdriven ODW; and –·–·–, weak ODW.

flow does not affect the C–J ODW. Another possibility is that the induction time would be increased enough to decouple the combustion process from the leading shock wave. Thus, a deflagration wave would be obtained downstream of the leading oblique shock wave. In the latter case, the combustion process could be extinguished by further expansion of the shocked gases, and the shock wave would become a Prandtl–Meyer wave farther downstream.

Previous experimental work on this type of interaction can be found in axisymmetric configurations only. Lehr[15] obtained a decoupled shock–deflagration system in hydrogen–air premixed flows over cone–cylinder models. These experiments clearly show that a deflagration is initiated near the tip of the cone and extends around the conical surface. Kasahara et al.,[16] studied conditions for which steady-state C–J detonation is obtained in hydrogen–oxygen premixed flow over cone–cylinder projectiles. In their experiments, when a steady detonation wave is obtained, the interaction between the overdriven ODW and the expansion that occurs at the projectile shoulder results in a C–J oblique detonation. More recently, Kasahara et al.,[17] examined the onset of combustion around spheres traveling at supersonic speeds in mixtures of oxygen and krypton burning acetylene, showing that critical conditions exist for the stabilization of Chapman–Jouguet oblique detonation waves. In this work, a critical sphere diameter relationship is proposed that is a function of the projectile velocity and drag coefficient and of the mixtures' Chapman–Jouguet velocity and cell width.

Numerical simultations of detonations induced by finite length wedges are found in the work of Papalexandris[18] and Pimentel et al.[11] The former work uses a global description for the combustion process, whereas the latter considers a detailed chemical kinetic mechanisms for hydrogen–air combustion. In both studies the choice of the freestream parameters and wedge angles led to C–J detonations only as the result of the interaction of the leading ODW and the expansion waves.

In this paper, the mathematical formulation of the problem and the numerical method used are presented first. Then results leading both to the formation of C–J ODW and to the decoupling between the leading OSW and the combustion process are presented. These results are analyzed on the basis of the characteristics of the flow and of the induction time of the chemical kinetic mechanism.

II. Governing Equations

In this work, where shock-triggered combustion of hydrogen–air mixtures in supersonic flows is studied, the two-dimensional Euler equations are used to decribe the flowfield. Neglecting molecular transport effects in this flowfield is a valid assumption outside the boundary layer that develops over the wedge surface.[19] Heat transfer by radiation is also neglected, because the products of combustion and the fuel–oxidizer mixture used may be considered as a transparent medium. Thus, in integral form, these equations can be expressed as

$$\iint_V \frac{\partial \boldsymbol{U}}{\partial t}\,\mathrm{d}x\mathrm{d}y + \int_S (\boldsymbol{F}\mathrm{d}y - \boldsymbol{G}\mathrm{d}x) = \iint_V \boldsymbol{Q}\,\mathrm{d}x\mathrm{d}y \tag{1}$$

where vectors $\boldsymbol{U}$, $\boldsymbol{F}$, $\boldsymbol{G}$, and $\boldsymbol{Q}$ are written as

$$\boldsymbol{U} = \begin{bmatrix} \rho \\ \rho u \\ \rho v \\ \rho E \\ \rho Y_1 \\ \rho Y_2 \\ \vdots \\ \rho Y_{N-1} \end{bmatrix}, \quad \boldsymbol{F} = \begin{bmatrix} \rho u \\ \rho u^2 + p \\ \rho uv \\ u(\rho E + p) \\ \rho Y_1 u \\ \rho Y_2 u \\ \vdots \\ \rho Y_{N-1} u \end{bmatrix}$$

$$\boldsymbol{G} = \begin{bmatrix} \rho v \\ \rho uv \\ \rho v^2 + p \\ v(\rho E + p) \\ \rho Y_1 v \\ \rho Y_2 v \\ \vdots \\ \rho Y_{N-1} v \end{bmatrix}, \quad \boldsymbol{Q} = \begin{bmatrix} 0 \\ 0 \\ 0 \\ 0 \\ \dot{\omega}_1 W_1 \\ \dot{\omega}_2 W_2 \\ \vdots \\ \dot{\omega}_{N-1} W_{N-1} \end{bmatrix} \tag{2}$$

In the equation system (1) and (2) ρ is density, u and v are Cartesian velocity components in directions x and y, E is total energy per unit mass, p is pressure, and Y_i, $\dot{\omega}_i$, and W_i are mass fraction, molar production rate, and molecular weight of the species i, respectively. The state equation for a mixture of thermally perfect gases

$$p = \rho \mathcal{R} T \sum_{i=1}^{N} \frac{Y_i}{W_i} \tag{3}$$

is used to evaluate the pressure p; in this equation $\mathcal{R}$ is the universal gas contant. The total energy E is defined as the sum of the internal energy and the kinetic energy,

$$E = e + \frac{1}{2}(u^2 + v^2) = \sum_{i=1}^{N} Y_i e_i + \frac{1}{2}(u^2 + v^2)$$

$$= \sum_{i=1}^{N} Y_i h_i - \frac{p}{\rho} + \frac{1}{2}(u^2 + v^2) \tag{4}$$

from which the temperature T is calculated.

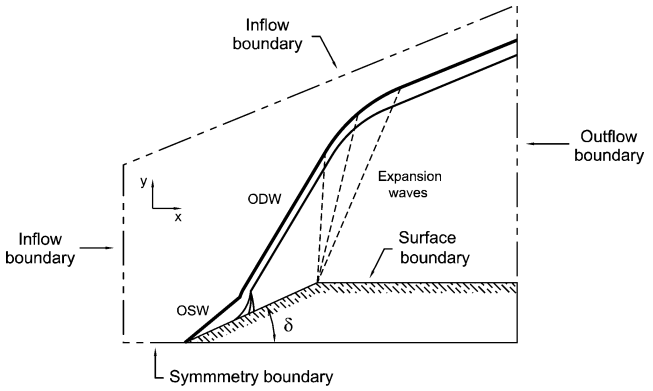

Fig. 3 Schematic representation of the computational domain and boundary conditions adopted.

In Eq. (1) only $N-1$ chemical species equations are needed, because the last species is calculated from the constraint

$$Y_N = 1 - \sum_{i=1}^{N-1} Y_i$$

The computations involving gas-phase chemistry and thermodynamic data are performed using the Chemkin-II package.[20,21]

The detailed kinetic chemical mechanism used is the one compiled by Balakrishnan and Williams,[22] which involves 9 species (H_2, O_2, H, O, OH, HO_2, H_2O_2, H_2O, N_2) and 21 elementary reactions. This mechanism has been used previously for the computation of OSW/ODW transitions.[7,11] A detailed description of the chemical process is required to capture the different characteristic timescales and their variations with the flow pressure and temperature.

Figure 3 shows the geometry of the computational domain. Flow enters the domain from the left through the inflow boundary in a direction that is parallel to the x axis, and leaves the domain at the right through the outflow boundary. Freestream values of Mach number, temperature, pressure, and mass fractions (M_∞, T_∞, p_∞, and $Y_{k\infty}$) are prescribed at the inflow boundary. At the ramp surface boundary, slip, adiabatic, noncatalytic boundary conditions are considered. Such a choice of boundary conditions does not allow the computation of the boundary layer that develops over the ramp surface. Thus, it is clearly expected that the ignition of the reactive mixture that may occur within the boundary layer[19] does not influence the development of the combustion process downstream of the OSW. The computational domain begins a small distance upstream of the leading edge of the ramp, which implies the presence of a symmetry plane. Symmetry conditions are imposed at this boundary. At the outflow boundary nonreflective characteristic boundary condition are used.[23]

III. Numerical Method

Computations are performed using a numerical code[24] that solves the governing equation system (1) and (2) using an upwind cell-centered finite volume method on unstructured triangular meshes. This code uses a time-step splitting scheme technique[25] that leads to second-order accuracy in time and separates the fluid dynamic evolution from the chemical evolution. A classical second-order Runge–Kutta technique is used to advance the fluid dynamic part in time, whereas a stiff ODE solver[26] is employed to integrate the chemical evolution. Concerning the spatial discretization, the interface fluxes are formulated using the advection upstream splitting method.[27] Higher order spatial accuracy is sought with monotonic upwind scheme for conservation laws (MUSCL)[28,29] extrapolation. However, tests performed on a simple advection problem show that the spatial order of accuracy achieved on a general triangular mesh is, at best, 1.4 (Ref. 30). To improve the resolution without incurring excessive computational penalties, mesh adaptation is performed using refinement[24] and coarsening[31] procedures.

IV. Results and Discussion

The computations presented here were performed for stoichiometric hydrogen–air mixtures using freestream Mach number $M_\infty = 8$ and pressure $p_\infty = 0.75$ atm. This Mach number was chosen because, as shown in Fig. 2, it yields a wide range of flow deflection angles (δ_{cj}, δ_{max}) for which stable ODW can be obtained.[7] For every computation performed, four mesh adaption passes were carried out. The chosen ramp length allows for a complete OSW/ODW transition, followed by the stabilization of an overdriven ODW, prior to the deflection of the surface. Each mesh adaption pass occurs after convergence of the solution, and triangles are refined where any of the primitive variables (p, u, v, T, Y_i) exceed 10% of its maximum variation on the flowfield. Even if the overall flowfield is in a steady-state, flow instabilities develop between the leading OSW and the thermal runaway region, which eventually lead to the formation of detonation cells. The structure of detonation cells, which is the object of research of several recent works, is outside the scope of this study.

The total CPU time for the resulting Fortran code exceeded 3 weeks, for any of the computed cases shown in this work, on a Pentium IV 2.4-MHz processor using Linux RedHat 8.0 distribution and the Gnu compiler. Although these long computational durations preclude the use of finer grid spacings, the results obtained with three refinement passes only led to the same overall flow structures as those presented here, albeit with an expected lesser level of detail concerning the detonation waves.

A. Formation of a Chapman–Jouguet Oblique Detonation Wave

The results of the interaction between an ODW and expansion waves for the case $\delta = 30$ deg, a ramp height of $h = 2.15$ mm, and $T_\infty = 275$ K are presented in Figs. 4–6. Note that results analogous to those presented here were obtained for $T_\infty = 300$ K. However, as identical flow structures are observed, these are not shown here. The range of flow deflection angles for stable detonations and the angle of the C–J ODW obtained from the polar analysis are (δ_{cj}, δ_{max}) = (14.9 deg, 41.8 deg) and $\theta_{cj} = 39.1$ deg, respectively. Thus, the wedge angle chosen is an intermediate angle in this range. The overdriven ODW angle, calculated by the same technique, is $\theta_{ODW} = 48.5$ deg. The final mesh contains 105,687 nodes and 210,532 volumes.

Figure 4 shows pressure, temperature, and OH mass fraction contours. In this figure the transition between the OSW and the ODW is observed over the wedge ramp. In the transition region the leading OSW is intercepted by the detonation wave that originates in the shocked gases region. The complex flow structure in this region has been examined in several previous numerical studies.[6,7] From the interaction region emanate an overdriven ODW, a reflected shock wave, an expansion wave, and a shear layer. This expansion wave, which deflects the flow downstream to the transition region so that streamlines are parallel to the x axis near the ramp surface, is responsible for the weakening of both the reflected shock wave and the overdriven ODW. This structure is in accordance with the work of Ghorbanian and Sterling,[32] which summarizes some of the possible flow structures when the interactions are quasi-one-dimensional and localized pockets of subsonic gases are absent. Note that the grid resolution in this region is 5 μm, which leads to the presence of at least 30 computational cells in the induction region of the chemical process. It can also be noted that the overdriven ODW is fully developed prior to its interaction with the expansion waves. This interaction leads to the progressive bending of the overdriven ODW. This bending seems to stop at a constant angle of $\theta_R \approx 39$ deg, which is close to the C–J ODW angle obtained with the polar technique $\theta_{cj} = 39.1$ deg. At the end of the interaction, the combustion process remains tightly coupled with the leading OSW. This result is similar to those obtained by Papalexandris[18] and Pimentel et al.[11] Figure 4 also shows that the interaction of the expansion fan and the shear layer that emanates from the triple point leads to the bending of both these flow structures.

Figure 5 shows magnified views of density and H mass fraction contours corresponding to a region of the flowfield where the C–J ODW is fully developed. The refined computational mesh is also

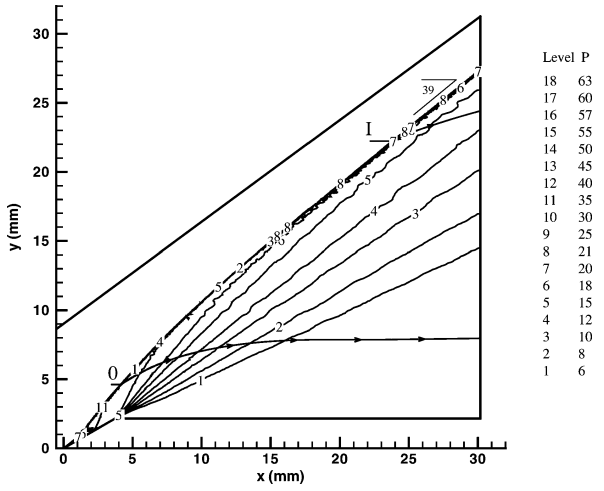

a) Overall flow structure: pressure

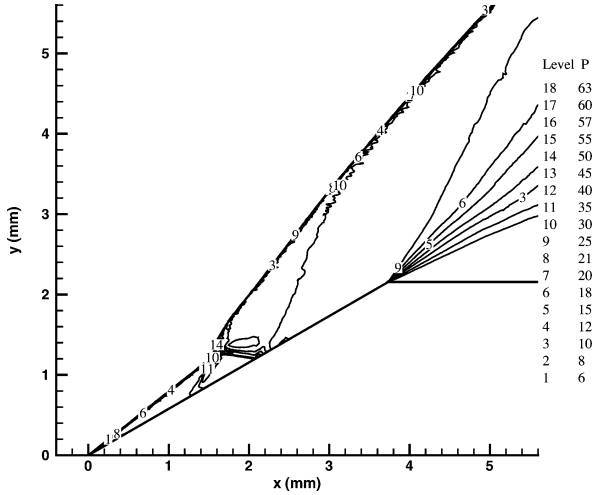

b) Transition region: pressure

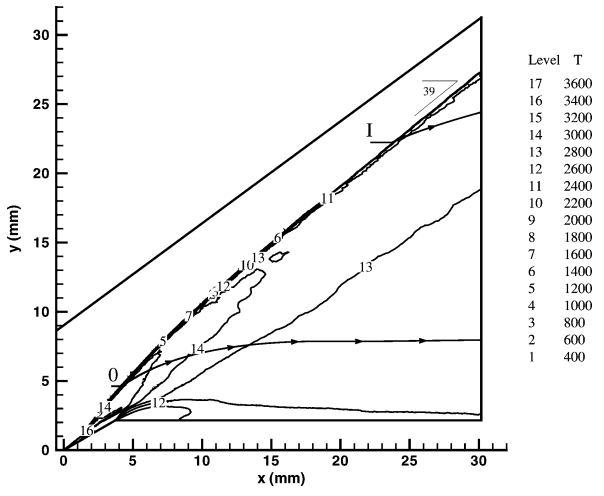

c) Overall flow structure: temperature

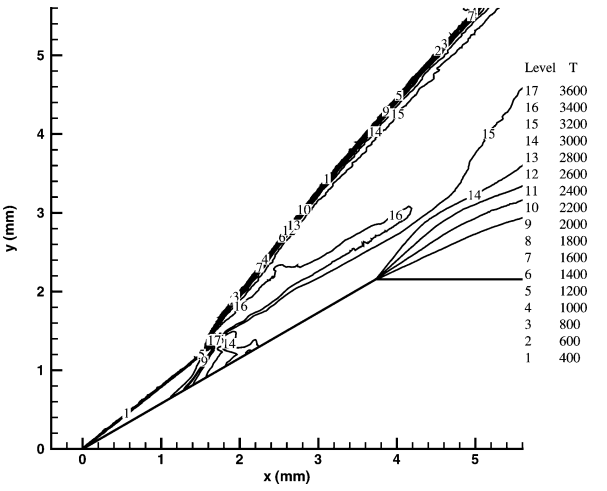

d) Transition region: temperature

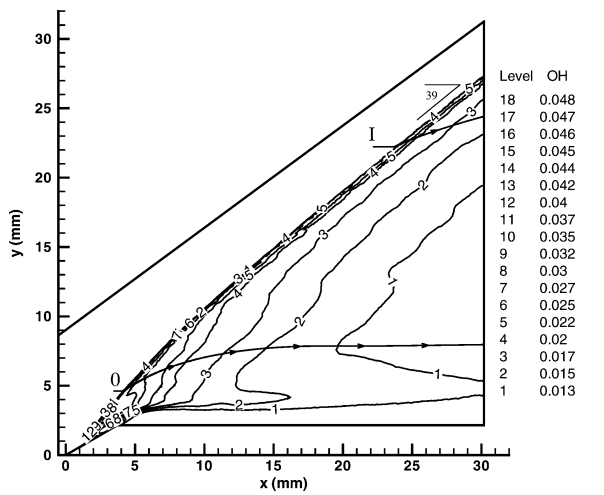

e) Overall flow structure: OH mass fraction

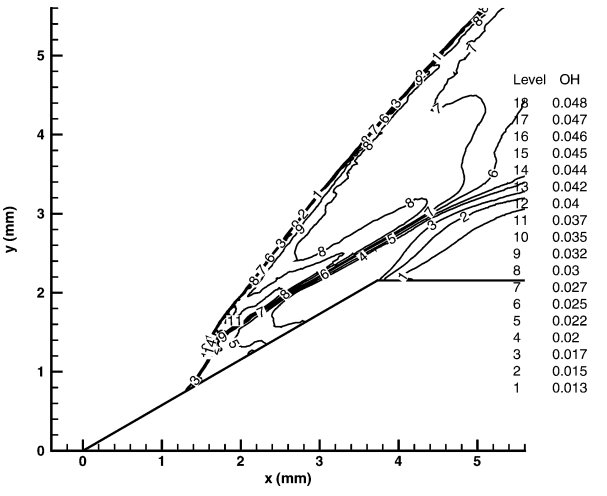

f) Transition region: OH mass fraction

Fig. 4 Contours of pressure (atm), temperature (K), and OH mass fraction; $\delta = 30$ deg, $M_\infty = 8$, $T_\infty = 275$ K, and $p_\infty = 0.75$ atm.

shown in this figure. Note that density and species concentration inhomogenieties indicate that instabilities are present in the computed flowfield.

Figure 6 shows the pressure, density, OH mass fraction, and temperature evolution along streamlines 0 and 1, which are also plotted in Fig. 4. Streamline 0 is plotted through the leading overdriven ODW, whereas streamline 1 passes through a region where the ODW presents the same angle as that of a C–J ODW. The peak pressures at the Zel'dovich, von Neumann, and Döring (ZND)[33] state predicted by the polar analysis for the overdriven and the C–J ODWs, 32.1 and 22.5 atm, are in excellent agreement with those given by the numerical computations, 31.5 and 22.0 atm, respectively. Moreover, the predicted pressure for the C–J state of the burned gases, 12.7 atm, is practically the same as the one computed, 13.5 atm, which indicates that the expansion of the burned gases, as depicted in this figure, is not fully achieved yet. In this figure it is also possible to

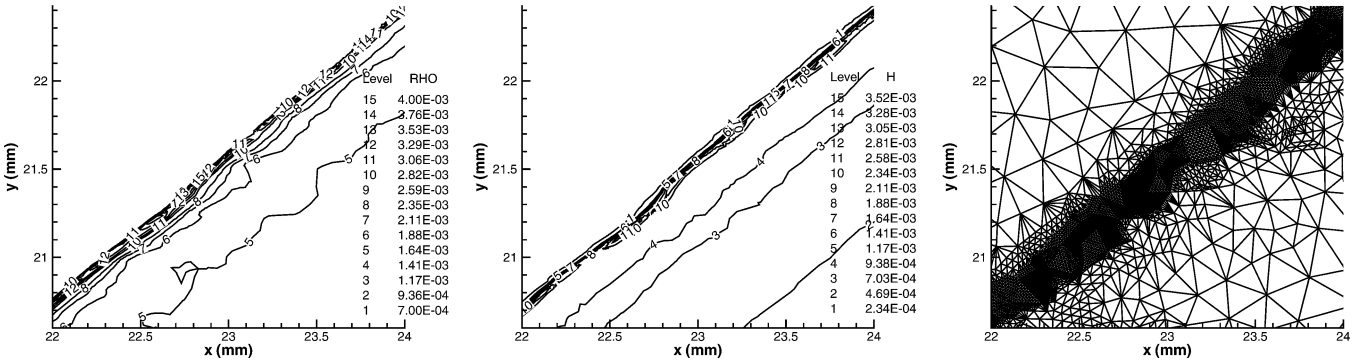

Fig. 5 Magnification of density (g/cm^3), H atom mass fraction fields, and computational mesh in the C–J ODW region of Fig. 4.

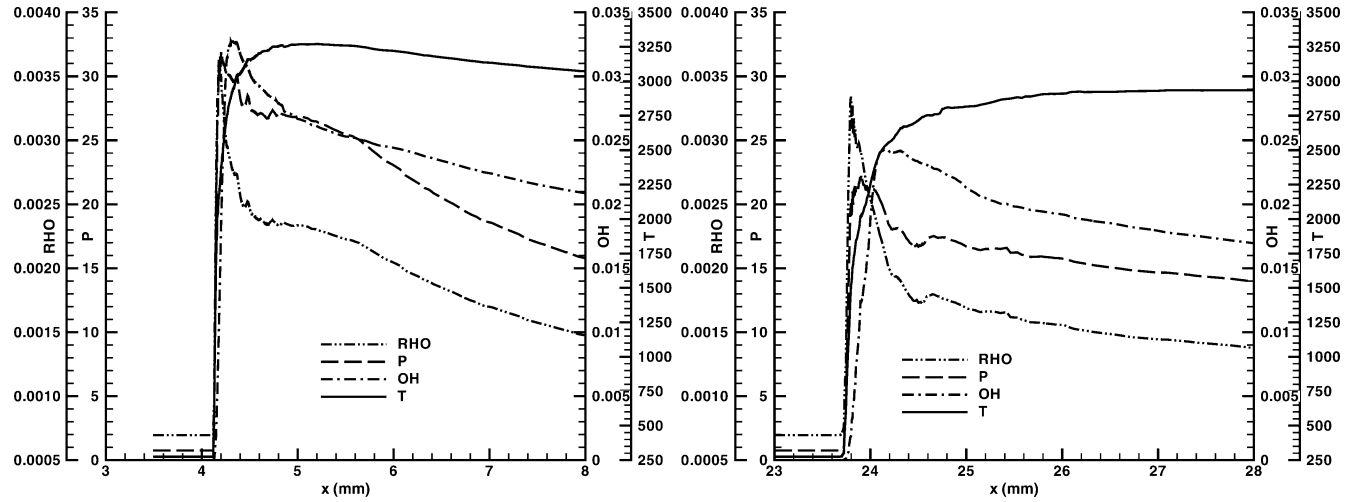

a) Streamline 0 **b) Streamline 1**

Fig. 6 Longitudinal evolutions of the density (g/cm^3), pressure (atm), OH mass fraction, and temperature (K) along selected streamlines plotted in Fig. 4.

observe the increment in the induction length from the overdriven ODW to the C–J ODW, which varies from 15 μm at the overdriven ODW to 25 μm at the C–J ODW. The characteristic grid size downstream of the overdriven ODW is $\approx$5 μm, thus leading to at least three mesh cells between the shock wave and the thermal runaway region.

B. Decoupling of the Oblique Detonation Wave

The results of the interaction between the overdriven ODW and the expansion waves for the case $\delta = 40$ deg, a ramp height of $h = 0.3$ mm, and for a freestream temperature of $T_\infty = 300$ K, are show in Figs. 7 and 8. Results analogous to those discussed here were also obtained for $T_\infty = 275$ K but, since the flowfield structures are similar, these are not shown here. The flow deflection angles range for stable detonations is $(\delta_{cj}, \delta_{max}) = (14.4 \text{ deg}, 43.3 \text{ deg})$. The final mesh contains 127,474 nodes and 254,167 volumes.

Contours of pressure, temperature, and OH mass fraction are given in Fig. 7. The OSW/ODW transition can be observed in this figure and is shown in a enlarged view. Because, due to the increased ramp angle, the Mach number downstream from the overdriven ODW is smaller than in the previous case, the interaction between the expansion waves and the ODW begins closer to the ramp deflection point. Farther downstream of the beginning of this interaction, a progressive separation of the OH front from the pressure front occurs. Note that the sudden jump of the pressure indicates the presence of an oblique shock wave, whereas the OH mass fraction evolution is characteristic of the combustion process heat release. In this figure the overdriven ODW angle is $\theta_{ODW} \approx 59.6$ deg, whereas the angle of the shock wave at the exit of the computational domain is $\theta_R \approx 27$ deg, which is smaller than the C–J ODW angle, $\theta_{cj} = 37.1$ deg, calculated by the polar technique. This computed value of θ_{ODW} is in excellent agreement with the one given by the polar analysis, 59.7 deg.

Selected streamlines are plotted in Fig. 7. Streamline 0 is plotted passing through the overdriven ODW, whereas streamline 1 is plotted through the point where the OSW has an angle equal to the C–J ODW, and streamline 2 is placed farther downstream, where the OSW angle is 32 deg. Figure 8 shows the evolution of pressure, density, OH mass fraction, and temperature along these streamlines. In this figure it can be observed that, in the region of the overdriven ODW, the heat release (OH evolution) occurs immediately downstream the leading OSW, which is an indication that the OSW is strongly coupled with the reaction front.

The evolution of selected flow properties for streamline 1, also shown in Fig. 8, clearly illustrates the increase in the distance between the OSW and the reaction front. The large increase of the induction length, which varies from 15 μm, along streamline 0, to 700 μm, along streamline 1, is sufficient to decouple the OSW from the reaction front. Note that, in these regions, the characteristic mesh spacing is on the order of 1 μm. As a consequence, at least 15 mesh cells lie at the induction region. Figure 8 also shows the properties evolution for streamline 2, where the decoupling of the OSW from the reaction front is completely evident. In this figure it can be seen that the maximum peak pressure at the ZND state varies from 44.0 atm at streamline 0 to 20.0 atm at streamline 1 to eventually 14.5 atm at streamline 2. When compared to the pressures of the ZND state computed by the polar technique at the overdriven and C–J waves, 42.8 and 20.6 atm, respectively, good agreement is obtained. However, one can observe that the decoupling process,

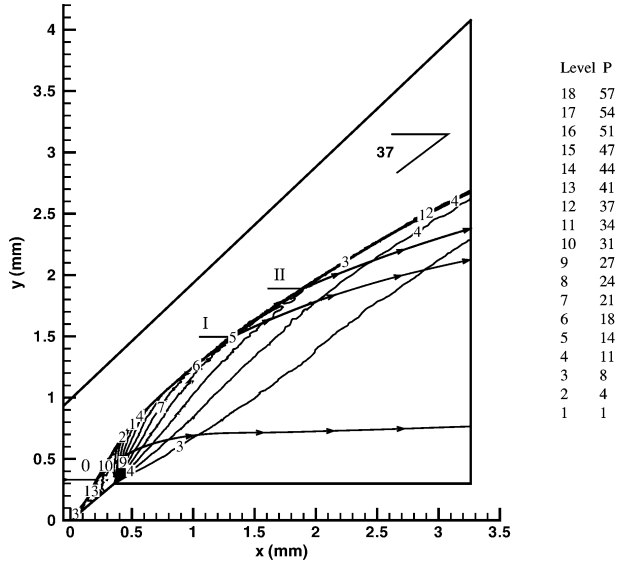

a) Overall flow structure: pressure

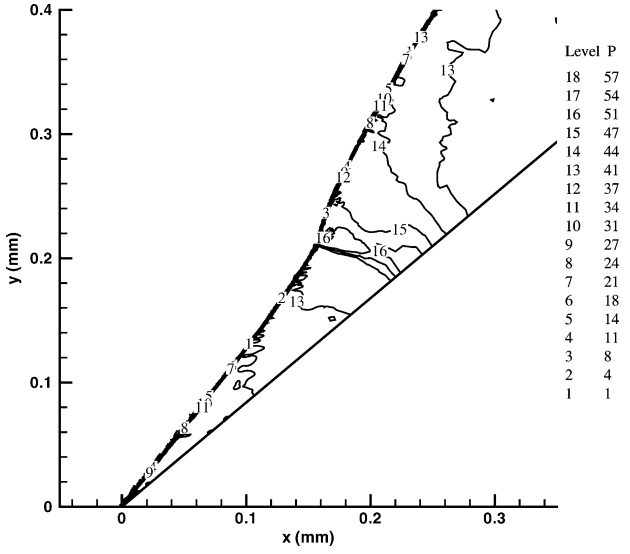

b) Transition region: pressure

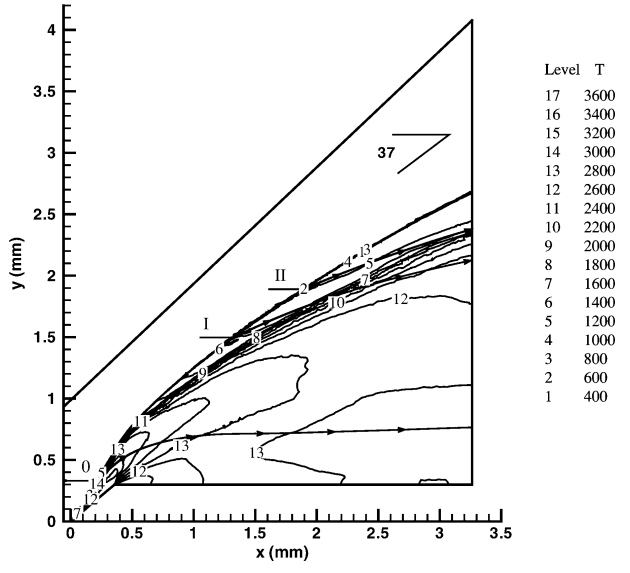

c) Overall flow structure: temperature

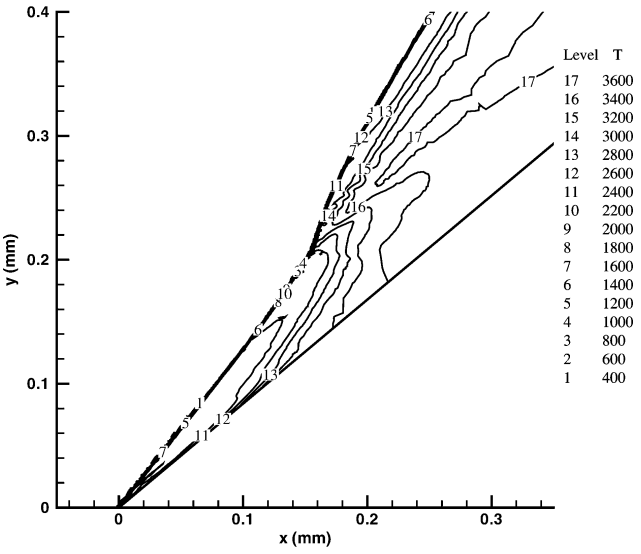

d) Transition region: temperature

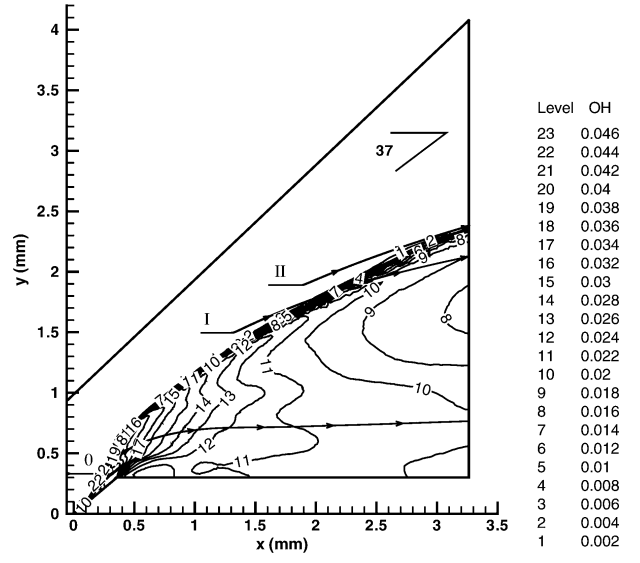

e) Overall flow structure: OH mass fraction

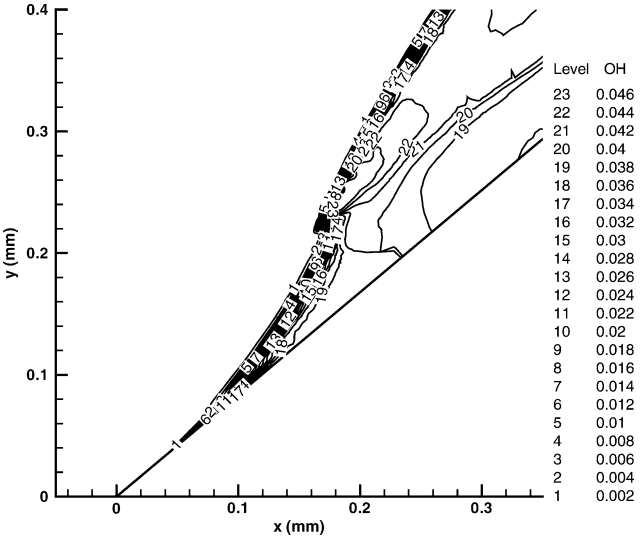

f) Transition region: OH mass fraction

Fig. 7 Contours of pressure (atm), temperature (K), and OH mass fraction; $\delta = 40$ deg, $M_\infty = 8$, $T_\infty = 300$ K, and $p_\infty = 0.75$ atm.

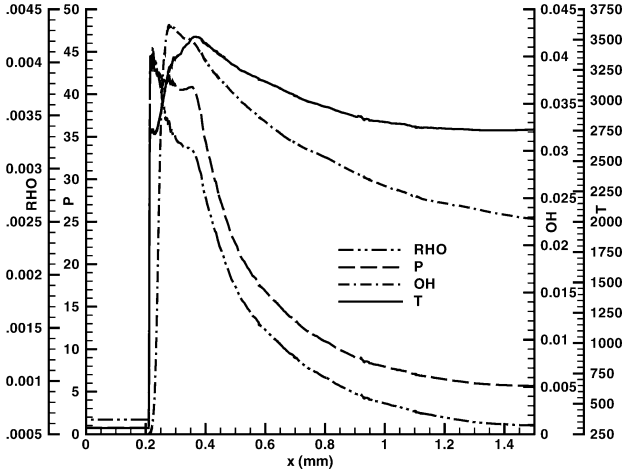

a) Streamline 0

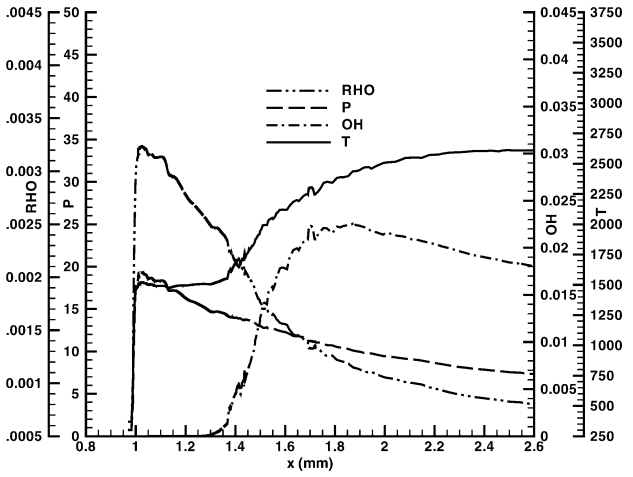

b) Streamline 1

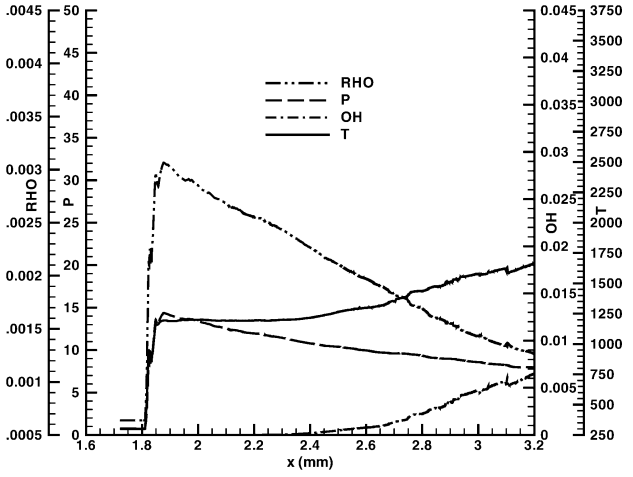

c) Streamline 2

Fig. 8 Longitudinal evolutions of the density (g/cm^3), pressure (atm), OH mass fraction, and temperature (K) along selected streamlines plotted in Fig. 7.

which is fully achieved in the region of streamline 2, is clearly evident at the region of streamline 1. This decoupling may be attributed to the strong flow expansion caused by the expansion fan, which is responsible for a decrease in the temperature and pressure of the shocked gases at the induction region. Because the induction length exhibits a strong sensitivity to small changes in the temperature due to the Arrhenius law, thus an increase of the induction length of the combustion process is the consequence of the decrease of the temperature and the pressure caused by the strong expansion of the shocked gases. Note that the computed pressure at a relatively large distance from the OSW through streamline 1, 8.5 atm, is considerably smaller than the one predicted for the C–J state, 11.7 atm.

C. Analysis of the Propagation of the Left-Running Characteristic

Figure 9 shows the left-running characteristic contours $C^+ = \arctan(v/u) + \arcsin(1/M)$. These characteristic lines represent the maximum angle with which a perturbation of the flow properties would travel, in a frame of reference fixed on the wedge. When a C–J ODW is obtained, at a given distance from the overdriven ODW, the value of C^+ is progressively decreased as the interaction between the ODW and the expansion occurs, which results in a shallower Mach cone locally. In the case shown in Fig. 9a, this process eventually leads to the isolation of the ODW by the line $C^+ = 39$ deg, which corresponds to a sonic surface that becomes parallel to the C–J ODW.

However, when decoupling between the combustion process and the leading OSW is observed, a different picture results, as can be verified in Fig. 9b. Indeed, downstream, the leading OSW, C^+, exhibits nonmonotonic behavior. Close to the OSW the value of C^+ decreases, and then increases through the reaction front and decreases subsequently in the burned gases region. The characteristic line $C^+ = 37$ deg, which has the same angle a C–J ODW would have, penetrates the induction region and merges with the leading

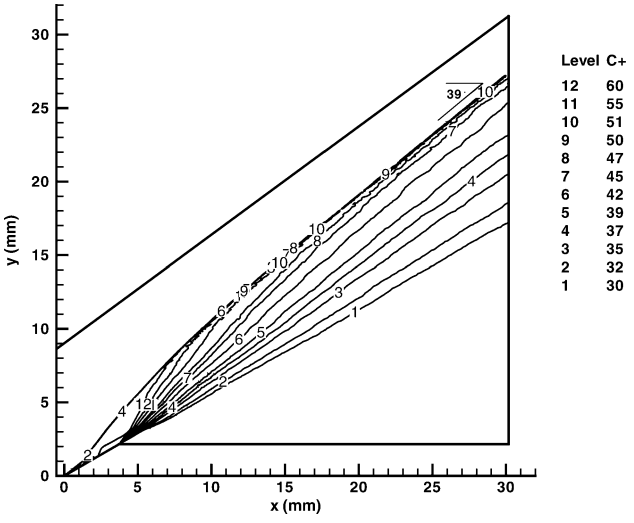

a) $\delta = 30$ deg, $T_\infty = 275$ K

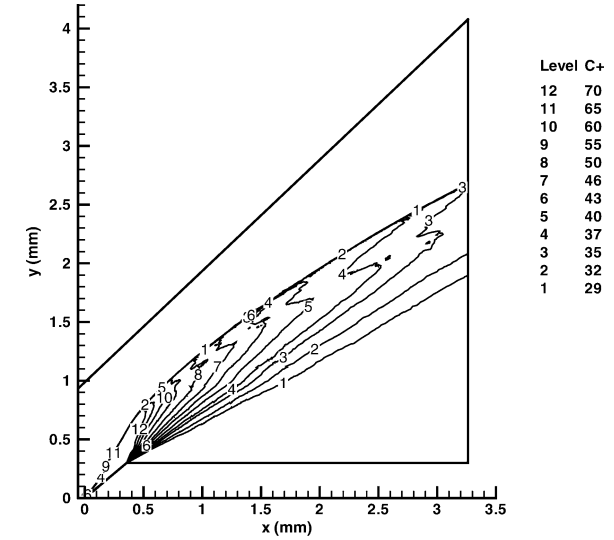

b) $\delta = 40$ deg, $T_\infty = 300$ K

Fig. 9 Contours of the left characteristic C^+, $M_\infty = 8$, and $p_\infty = 0.75$ atm.

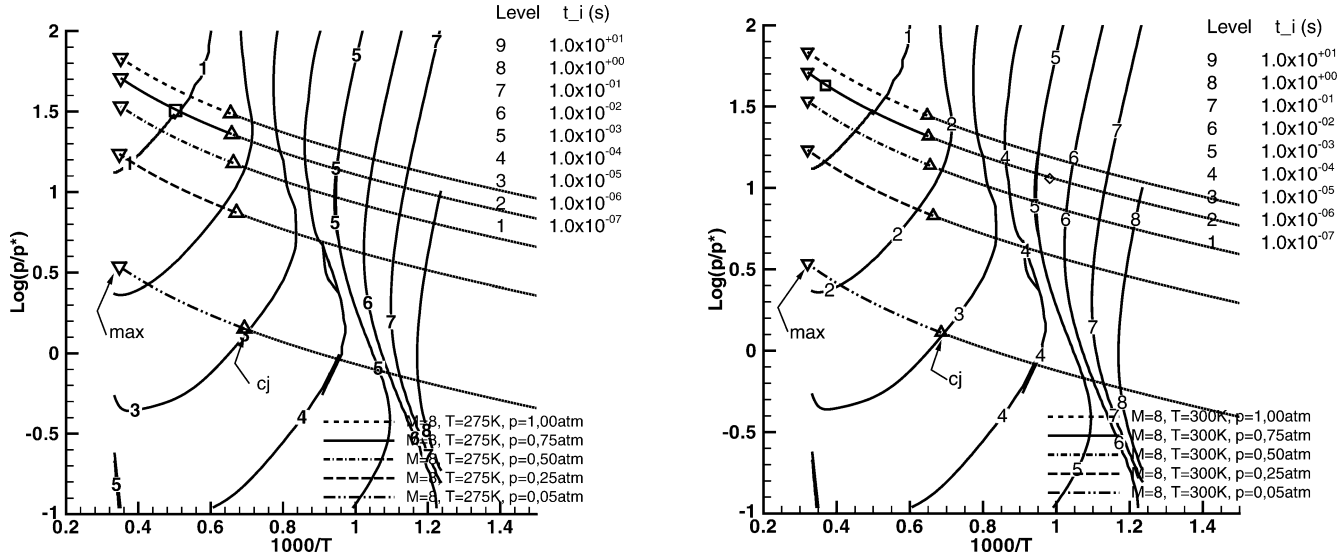

a) $T_\infty = 275$ **K** **b)** $T_\infty = 300$ **K**

Fig. 10 Lines of constant induction time for a stoichimetric hydrogen–air mixture (solid lines) and lines representative of the thermodynamic states of gases downstream the leading OSW for stabilized ODW over wedges ($p^* = 1$ atm) as a function of the temperature (K) and the pressure (atm): $\bigtriangledown$, $\delta = \delta_{max}$ and $\bigtriangleup$, $\delta = \delta_{cj}$.

OSW. As a consequence, the expansion fan is allowed to weaken this OSW, which leads to the observed increase on the induction length of the chemical process.

D. Analysis of the Induction Time

Figure 10 shows the lines of constant induction time t_i for hydrogen–air mixtures as a function of the initial temperature and pressure. The induction time is defined as the duration corresponding to 10% of the total temperature increase, calculated for the adiabatic thermal explosion at constant pressure (Semenov explosion[34]). In this figure the thermodynamic states of the shocked gases downstream from the leading OSW, which are part of the detonation structure, are also given for stable ODW over wedges. One should note that it is considered here that the ignition of the reactive mixture occurs for the conditions prevailing in the ZND state, which is a crude approximation that does not account for the actual behavior of the shocked gases within the detonation wave. The state of the shocked gases is plotted using the values obtained by the polar technique. The left limits ($\bigtriangledown$) of the lines correspond to the maximum flow deflection angles, δ_{max}, whereas the the symbol $\bigtriangleup$ denotes the Chapman–Jouguet state, that is, $\delta = \delta_{cj}$. In this figure, it can be observed that flow expansion leads to a reduction in pressure and temperature, which in turn increases the value of the induction time.

For the case in which a C–J ODW is obtained, the induction time variation along the ODW, calculated with the pressure and temperature values downstream from the leading OSW determined by the polar technique, is shown in Fig. 10a. The induction time is found to increase from $\approx$90 ns ($\square$) at the overdriven ODW to $\approx$500 ns ($\bigtriangleup$) at the C–J ODW.

Figure 10b shows the computed induction time t_i variation when decoupling of the combustion process is observed downstream the OSW. When the pressure and temperature of the shocked gases vary from (2703 K, 42.95 atm), downstream from the overdriven ODW, to (1017.5 K, 11.5 atm) downstream from the OSW at the exit of the computational domain, the induction time of the thermal explosion t_i increases from 28 ns ($\square$) to 2.6 ms ($\diamond$). This increase in the induction time of five orders of magnitude is connected to the decoupling of the ODW.

V. Conclusions

A numerical study was performed to evaluate parameters that lead to Chapman–Jouguet oblique detonation waves as a result of the interaction between the overdriven ODW and expansion waves in stoichiometric hydrogen–air mixtures. Simulations were performed for freestream parameters $M_\infty = 8$, $p_\infty = 0.75$ atm, and two values of temperatures $T_\infty = 275$ and 300 K. Intermediate wedge angles within the range of flow deflection angles that support stable ODW (δ_{cj}, δ_{max}) led to the formation of Chapman–Jouguet oblique detonation waves. In this case, the left-running characteristic $C^+ = \arctan(v/u) + \arcsin(1/M)$, which has the same angle as C–J ODW, isolates the resulting ODW and further flow expansions do not affect it. For wedge angles near to the maximum flow deflection angle that permit stable detonations, δ_{max}, a decoupling of the reaction front from the oblique shock wave is observed. In this case, it is expected that further flow expansion would lead to the extinction of the combustion process and, eventually, the oblique shock wave would become a Prandtl–Meyer wave. The physical mechanisms that lead either to a C–J ODW or to combustion decoupling are still unknown. It has been observed, though, that when the decoupling occurs, the flow expansion leads to strong flow curvatures in the interaction region. Thus, the two-dimensional nature of the interaction should not allow a description of the detonation process by a quasi-one-dimensional polar technique.

The C–J measured value of the detonation cell width, λ, of the computed mixtures is around 6–8 mm (Ref. 8). It is interesting to note that, when decoupling occurs, the ratio between the height of the ramp h and induction length l_i (and thus of λ) of the chemical process downstream from the leading OSW of the overdriven ODW is smaller than when a C–J ODW is obtained. For given values of the induction length and ODW angle, the ramp height controls the pressure gradient of the expansion fan downstream from the ODW. Future work should be directed toward examining the influence of the ramp height on the decoupling process for a given ODW. Moreover, it would be interesting to perform analytical studies together with numerical simulations to understand the physical mechanisms that lead either to a C–J ODW or to a decoupled OSW–deflagration system. To this end, asymptotic techniques,[3] assuming high activation energy of the chemical reaction, seem to be a promising avenue. Further mesh refinement, beyond the limits of the available computational resources, would be desirable to fully capture the detailed structure of the detonation waves. Also, the development of higher order numerical schemes in unstructured meshes, currently under way, should result in better resolution of the inner detonation structure.

Acknowledgments

M. A. T. Walter thanks FAPERJ (Fundação Carlos Chagas Filho de Amparo à Pesquisa do Estado do Rio de Janeiro) for his scholarship. During this work L. F. Figueira da Silva was on leave from the Laboratoire de Combustion et de Détonique, Centre Nacional de la Recherche Scientifique, France, with a PROFIX scholarship from CNPq-Brazil.

References

[1]Hertzberg, A., Bruckner, A. P., and Bogdanoff, D. W., "Ram Accelerator: A New Chemical Method for Accelerating Projectiles to Ultrahigh Velocities," *AIAA Journal*, Vol. 26, No. 2, 1988, pp. 195–203.

[2]Heiser, W. H., Pratt, D. T., Daley, D. H., and Mehta, U. B., *Hypersonic Airbreathing Propulsion*, AIAA Education Series, AIAA, Washington, DC, 1994.

[3]Clavin, P., "Premixed Combustion and Gas Dynamics," *Annual Review of Fluid Mechanics*, Vol. 26, 1994, pp. 321–352.

[4]Smeets, G., "The Ram Accelerator: Perspectives and Experimental Results Already Achieved," *IUTAM Symposium on Combustion in Supersonic Flows*, edited by M. Champion and B. Deshaies, Kluwer Academic, Dordrecht, The Netherlands, 1997, pp. 219–236.

[5]Menees, G. P., Adelman, H. G., and Cambier, J. L., "Analytical and Experimental Investigation of the ODWE Concept," *AGARD PEP 75th Symposium Hypersonic Combined Cycle Propulsion*, 1990, p. 26.

[6]Li, C., Kailasanath, K., and Oran, E. S., "Detonation Structures Behind Oblique Shocks," *Physics of Fluids*, Vol. 6, No. 4, 1993, pp. 1600–1611.

[7]Figueira da Silva, L. F., and Deshaies, B., "Stabilization of an Oblique Detonation Wave by a Wedge: A Parametric Numerical Study," *Combustion and Flame*, Vol. 121, No. 4, 2000, pp. 152–166.

[8]Ciccarelli, G., Ginsberg, T., Boccio, J., Economos, C., Sato, K., and Kinoshita, M., "Detonation Cell Size Measurements and Predictions in Hydrogen-Air-Steam Mixtures at Elevated Temperatures," *Combustion and Flame*, Vol. 99, No. 2, 1994, pp. 212–220.

[9]Pratt, D. T., Humphrey, J. W., and Glenn, D. E., "Morphology of Standing Obique Detonation Waves," *Journal of Propulsion and Power*, Vol. 7, No. 5, 1991, pp. 837–845.

[10]Viguier, C., Guerraud, C., and Desbordes, D., "H_2–Air and CH_4–Air Detonations and Combustions Behind Oblique Shock Waves," *Twenty-Fifth Symposium (International) on Combustion*, Combustion Inst., Pittsburgh, PA, 1994, pp. 53–59.

[11]Pimentel, C. A. R., Azevedo, J. L. F., Figueira da Silva, L. F., and Deshaies, B., "Numerical Study of Wedge Supported Oblique Shock Wave–Oblique Detonations Wave Transitions," *Journal of the Brazilian Society of Mechanical Sciences*, Vol. 24, No. 3, 2002, pp. 149–157.

[12]Viguier, C., Gourara, A., and Desbordes, D., "Three-Dimensional Structure of Stabilization of Oblique Detonation Wave in Hypersonic Flow," *Twenty-Seventh Symposium (International) on Combustion*, Combustion Inst., Pittsburgh, PA, 1998, pp. 3023–3031.

[13]Morris, C. I., Kamel, M. R., and Hanson, R. K., "Expansion Tube Investigation of Ram-Accelerator Projectile Flowfields," AIAA Paper 96-2680, July 1996.

[14]Viguier, C., Figueira da Silva, L. F., Desbordes, D., and Deshaies, B., "Onset of Oblique Detonation Waves: Comparison Between Experimental and Numerical Results for Hydrogen–Air Mixtures," *Twenty-Sixth Symposium (International) on Combustion*, Combustion Inst., Pittsburgh, PA, 1996, pp. 3023–3031.

[15]Lehr, H. F., "Experiments on Shock-Induced Combustion." *Astronautica Acta*, Vol. 17, Nos. 4–5, 1972, pp. 589–597.

[16]Kasahara, J., Fujiwara, T., Endo, T., and Arai, T., "Chapman–Jouguet Oblique Detonation Structure Around Hypersonic Projectiles," *AIAA Journal*, Vol. 39, No. 8, 2001, pp. 1553–1561.

[17]Kasahara, J., Arai, T., Chiba, S., Takazawa, K., Tanahasi, Y., and Matsuo, A., "Criticality for Stabilized Oblique Detonation Waves Around Spherical Bodies in Acetylene/Oxygen/Kripton Mixtures," *Proceedings of the Combustion Institute*, Vol. 29, No. 2, 2002, pp. 2817–2824.

[18]Papalexandris, M. V., "A Numerical Study of Wedge-Induced Detonations," *Combustion and Flame*, Vol. 120, No. 4, 2000, pp. 526–538.

[19]Figueira da Silva, L. F., Deshaies, B., and Champion, M., "Numerical Study of Ignition within Hydrogen–Air Supersonic Boundary Layers," *AIAA Journal*, Vol. 31, No. 5, 1993, pp. 884–890.

[20]Kee, R. J., Rupley, F. M., and Miller, J. A., "Chemkin-II: A Fortran Chemical Kinetics Package for the Analysis of Gas-Phase Chemical Kinetics," Sandia National Labs., SAND89-8009B, Livermore, CA, April 1994.

[21]Kee, R. J., Rupley, F. M., and Miller, J. A., "The Chemkin Thermodynamic Database," Sandia National Labs., SAND87-8215B, Livermore, CA, April 1994.

[22]Balakrishnan, G., and Williams, F. A., "Turbulent Combustion Regimes for Hypersonic Propulsion Employing Hydrogen–Air Diffusion Flames," *Journal of Propulsion and Power*, Vol. 10, No. 3, 1993, pp. 434–436.

[23]Thompson, K. W., "Time Depedent Boundary Conditions for Hyperbolic Systems," *Journal of Computational Physics*, Vol. 68, No. 1, 1987, pp. 1–24.

[24]Figueira da Silva, L. F., Azevedo, J. L. F., and Korzenowski, H., "Unstructured Adaptive Grid Flow Simulations of Inert and Reactive Gas Mixtures," *Journal of Computational Physics*, Vol. 160, No. 2, 2000, pp. 522–540.

[25]Strang, G., "On the Construction and Comparison of Difference Schemes," *SIAM Journal of Numerical Analysis*, Vol. 5, 1968, pp. 506–517.

[26]Byrne, G. D., and Dean, A. M., "The Numerical Solution of Some Kinetics Models with VODE and CHEMKIN II," *Computers and Chemistry*, Vol. 13, No. 3, 1993, pp. 297–302.

[27]Liou, M.-S., "A Sequel to AUSM: AUSM$^+$," *Journal of Computational Physics*, Vol. 129, No. 2, 1996, pp. 364–382.

[28]Hirsch, C., *Numerical Computations of Internal and External Flows*, Wiley, Chichester, England, U.K., 1990.

[29]Venkatakrishnan, V., "Convergence to Steady State Solutions of the Euler Equations on Unstructured Grids with Limiters," *Journal of Computational Physics*, Vol. 118, No. 1, 1995, pp. 120–130.

[30]Azevedo, J. L. F., Strauss, D., and Figueira da Silva, L. F., "An Order of Accuracy Analysis for Flux-Vector Splitting Schemes on Unstructured Grids," *15th Brazilian Congress of Mechanical Engineering* [CD-ROM], Brazilian Society of Mechanical Engineering and Sciences, Rio de Janeiro, Brazil, 1999.

[31]Walter, M. A. T., Abdu, A. A. Q., Figueira da Silva, L. F., and Azevedo, J. L. F., "Evaluation of Adaptative Mesh Refinement and Coarsening for the Computation of Compressible Flows on Unstructured Meshes," *International Journal for Numerical Methods in Fluids*, Vol. 49, No. 9, 2005, pp. 999–1014.

[32]Ghorbanian, K., and Sterling, J. D., "Influence of Formation Processes on Oblique Detonation Wave Stabilization," *Journal of Propulsion and Power*, Vol. 12, No. 3, 1996, pp. 509–517.

[33]Fickett, W., and Davies, W. C., *Detonation: Theory and Experiment*, Dover, Mineola, NY, 2000.

[34]Zeldovich, Y. B., Barenblatt, G. I., Librovich, V. B., and Makhviladze, G. M., *The Mathematical Theory of Combustion and Explosions*, Consultants Bureau, New York, 1985.

M. Sichel
Associate Editor